An Acad Bras Cienc (2021) 93(1): e20190322 DOI 10.1590/0001-3765202120190322
Anais da Academia Brasileira de Ciências | *Annals of the Brazilian Academy of Sciences*
Printed ISSN 0001-3765 I Online ISSN 1678-2690
www.scielo.br/aabc | www.fb.com/aabcjournal

GEOSCIENCES

Integration of multisources data for quarry slope stability assessment in the Itaoca district (Southeastern Brazil)

MARCOS EDUARDO HARTWIG & CÉSAR AUGUSTO MOREIRA

Abstract: Usually, stability conditions of excavation slopes are evaluated by means of kinematic analysis and geomechanical classification systems. However, field surveys are concentrated at the slope toe and information about the upper and internal portions of rock masses are not taken into account. In order to tackle with these issues multisources data were integrated. The studies were carried out in a marble quarry located in one of the largest Brazilian poles of dimension stones. Results have shown that drone images actually help in the structural characterization of rock masses because they allow to classify variable degrees of fracturing and to identify structural domains in the entire slope face. In addition, the number of discontinuities interpreted from drone images was much larger than that determined by scanline survey methods. This demonstrates that the subsampling of classical survey methods may significantly affect slope stability assessment. Results have also shown that the intensive use of explosives as a method for rock dismantling was an important mechanism of fracture generation. The electrical resistivity tomography method coupled with the other survey methods employed in this work, proved an important tool for rock mass characterization and quarry exploitation, since it allowed identifying and assessing subsurface fractured zone.

Key words: drone remote sensing, electrical resistivity tomography, kinematic analysis, Rock Mass Rating, structural survey.

INTRODUCTION

Mine slopes are intrinsically subjected to instabilizations, which can lead to human lifes and equipment losses or the momentaneous interruption of mine production. They depend on slope geometry (height x inclination), degree of chemical weathering, lithotypes, discontinuity properties, groundwater, field stress, seismic loadings and blasting (Hoek & Bray 1981, Wyllie & Mah 2004, Read & Stacey 2009).

Among these factors, discontinuities are perhaps, the most intervening factor on rock slope instabilities. Depending on the geometrical relationship between discontinuity sets and slope orientation, four failure modes can be defined: planar, wedge and toppling (both flexural and direct) (Alejano et al. 2017, Kliche 1999, Hudson & Harrison 1997, Goodman 1980). The kinematic slope stability analysis comprise the identification of the most probable failure modes by means of stereographic projections (Park et al. 2016). Although kinematic slope stability method is not able to lead to the determination of a factor of safety, it does provide a fast analysis of the feasibility of movement along joint planes. Rock slope stability conditions can also been assessed by means of geomechanical classifications. They are based on the assignment of grades for

descriptive geomechanical parameters, which will define classes of rock mass quality with unique strength and deformability parameters. Each one of these rock mass classes will behave distinctively and will affect to a greater or lesser degree the stability of rock slopes (Basahel & Mitri 2017, El-Naqa 1994, Bieniawski 1989, Romana 1985, Barton et al. 1974). Both approaches involve field inspections at sampling stations distributed along slope faces (ISRM 1981, Herget 1977, Gyenge & Herget 1977). However, one of the main difficulties is due to the concentration of data samples in the lower portion of the slope (usually 1st third), while the upper portion are neglected due to access issues. In addition, sampling only comprises the characterization of the exposed surfaces (outcrops). Therefore, information about the subsurface conditions are compromised, being eventually supplied by a dense mesh of geotechnical drillings. In recent years, there has been a broad and growing advance in the use of geophysical tools such as electrical resistivity tomography (ERT) and drone remote sensing for geological, structural, hydrogeological and geotechnical characterization of rock masses (Tziavou et al. 2018, Chambers et al. 2015, Carrière et al. 2013, Carrozzo et al. 2008). These tools are relatively inexpensive, versatile, and provide surface and subsurface data with a very high detail scale (> 1: 500).

The study area is located in the Espírito Santo state, southeastern Brazil, a region that includes hundreds of quarries and open pits for the exploitation of dimension stones, Portland cement as well as aggregates for civil construction industry. In 2017, the Espírito Santo state contributed with up to 36.9 % of the Brazilian dimension stone production (Abirochas 2018). The study area is located in the district of Itaoca, southern region of the state of Espírito Santo. It comprises an inactive marble quarry, exploited for the production of materials for both the civil construction and steel industries. In view of the above, the aim of this work is to integrate data collected by different sources for the purpose of rock slope stability assessment, such as high resolution drone photographs, geological and structural field surveys, geomechanical classification of rock masses and electrical resistivity prospecting.

Study area

The study area has a mining area of 0.3 km2 and depth of approximately 56 meters (Figure 1). It has five (5) benches with approximately 10 meters height each. The deeper portion of the quarry is submerged (elevation 199 m.a.s.l) and the uppermost slope (elevation 255 m.a.s.l) is composed of redish lateritic soil and for this reason both of them were not investigated. The quarry southeast flank consists of a single high slope of 40 meters high. Debris of excavation are observed in all benches.

In the southern region of the state of Espírito Santo outcrops rocks belonging to the Paraíba do Sul Complex included in the Araçuaí Belt of Neoproterozoic age striking N-S. The Paraíba do Sul Complex was invaded by late to post-tectonic magmatism and crossed by the Batatal and Guaçuí dextral shear zones (Pedrosa-Soares & Wiedmann-Leonardos 2000, Silva 1993). It consists of para-derived metamorphic rocks, mainly kinzigitic gneisses, intercalated with amphibolites, quartzites, marbles and calcissilicatic rocks. Metamorphic grades varies from greenschist up to granulite facies.

In the study area outcrops massive and banded calcitic white marbles, cut by fresh to very weathered dikes of metamafic (amphibolites) and granitic rocks (Jordt-Evangelista & Viana 2000). It is worth mentioning that only one dike of granitic rock was mapped throughout the quarry area. The contact between dikes and marbles

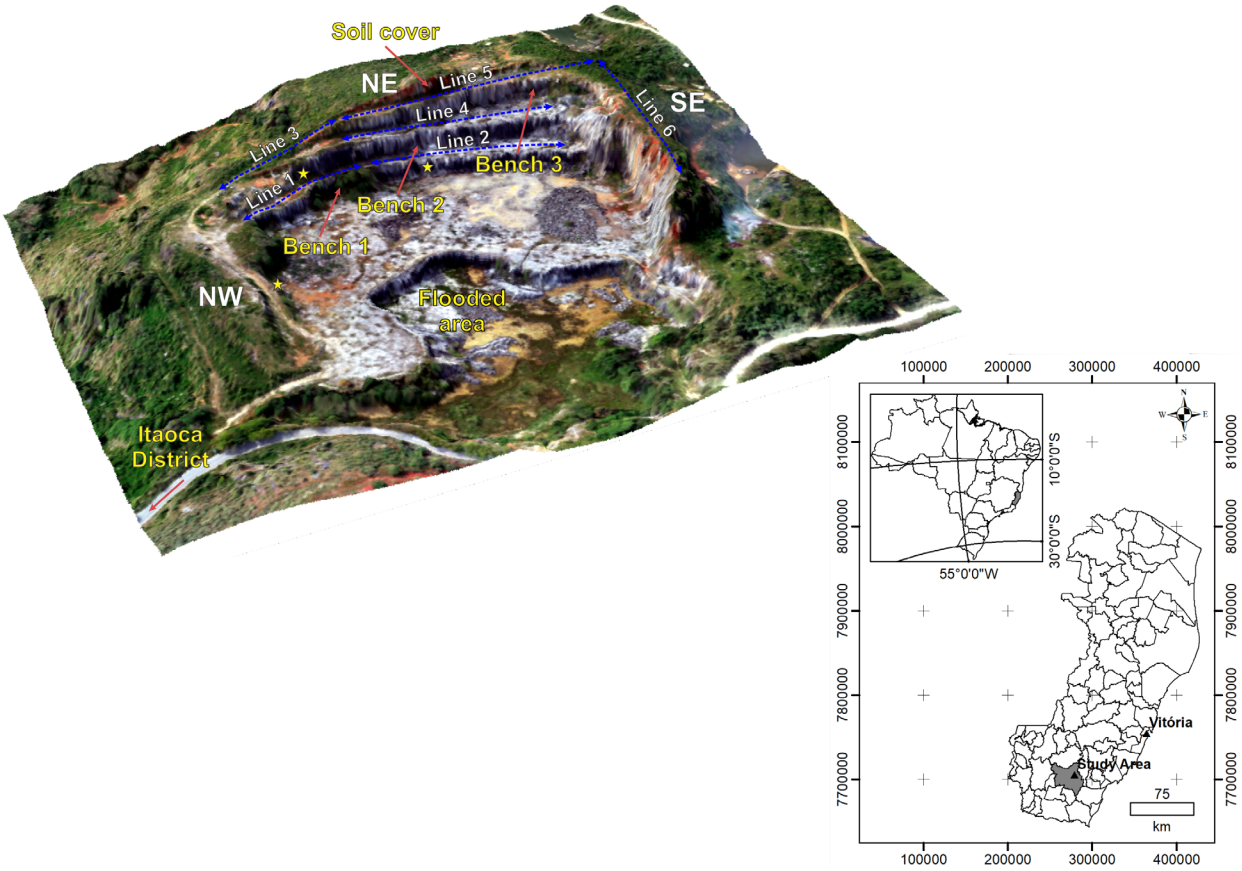

Figure 1. **Location of the study area: to the left, quarry geometric and topographical features and adopted nomenclature, with indication of the electrical geophysical survey lines. Yellow stars indicate places where rock failures have been observed. For details, consult the text.**

can exhibit greenish scarns of few centimeters thick. Banded marbles are characterized by both the intercalation of light and dark bands or by the intercalation of medium and very course-grained marbles. Dark bands have few milimeters thick and seems to correspond to impurities (Santos & Hartwig 2018) (Figura 2). Banded marbles such as the one depicted in Figure 2b were observed mainly in the NW Slope.

MATERIALS AND METHODS

The methodology adopted in this work was based in the following steps: (1) drone flyover with the purposes of acquiring updated aerial photographs with high spatial resolution and performing a topographic survey of the study area. These piece of information were used for structural analysis and as a georeferenced basemap; (2) kinematic slope stability analysis; (3) geomechanical characterization by using the Rock Mass Rating – RMR classification system (Bieniawski 1989); and (4) geophysical survey by employing the electrical resistivity tomography method (Daily et al. 2005).

For the generation of the digital elevation model (DEM), obtaining orthophoto mosaic and photographs of slope faces, an aerial survey was carried out with a Drone Quadcopter (DJI Phantom 4 – Professional) equipped with Gimbal stabilizer, 20 Megapixel camera

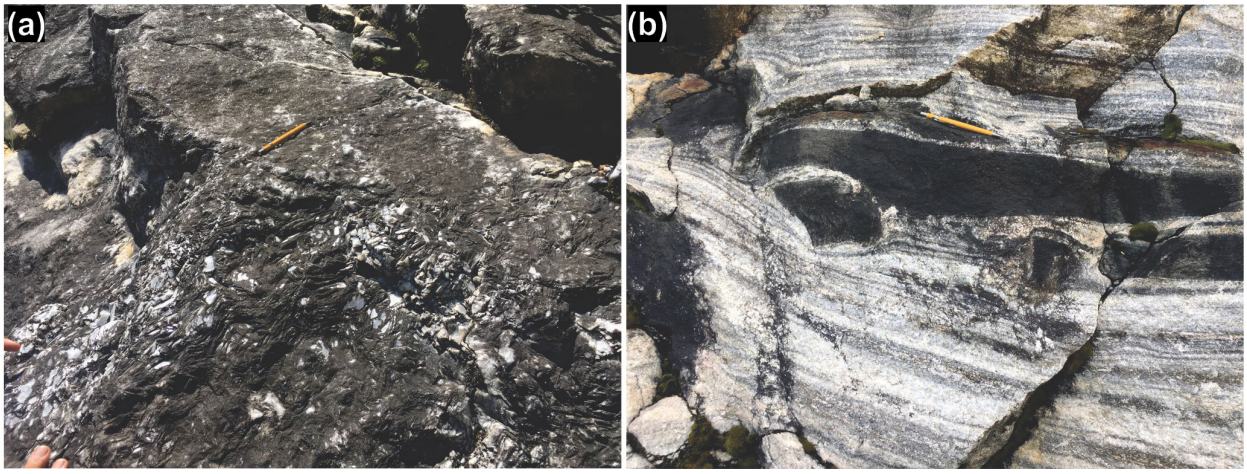

Figure 2. Main lithotypes found in the study area: (a) very course-grained marble showing massive structure; and (b) banded marble cut by dismembered metamafic dikes.

resolution and radio control. The flight was performed in a sunny day on March 03, 2018 in an autonomous fashion at a height of 120 meters with an approximate flight time of 8', with 80% of forward overlap and 70% of sidelap, totaling 117 pictures. The data collected were processed in the Agisoft Photoscan software. The average ground sample distance (GSD) is 3.77 cm/pixel. No ground control point (GCP) was acquired for the evaluation of the X-Y-Z accuracy. The horizontal datum used was the SIRGAS2000 and the map projection the Universal Transverse Mercator - UTM. In order to evaluate the effect of fracturing on the entire slope, slope face images were visually interpreted (through fracture digitalization), and fracture density maps were prepared in the ArcGIS software (ESRI 2015) using the kernel density tool. For the generation of these maps a search radius of 100 was used and the output area density unit was set to Square meters.

The kinematic slope stabiliy analysis consisted in the identification of planar and wedge failure modes. Toppling failure was not considered in this study, since it is very unlikely in marble cut slopes due to the rock properties itself and because this failure mode was not observed during fieldwork. For this purpose, it was performed a structural survey and discontinuities were treated by using stereograms (Hudson & Harrison 1997, Goodman 1980). For this purpose, the lower-hemisphere of the Schmidt-Lambert net was used. The field survey was conducted in March 2018 and lasted four (4) days. The scanline compass-based approach for discontinuity mapping was employed. Scanlines with 37 m long was arbitrarily chosen. Only structures with persistence greater than two (2) meters were considered, since they have greater potential of inducing rock failures. It was adopted the dip direction/dip geological convention for discontinuity description. The joint roughness (Jr) and the joint alteration (Ja) indexes were evaluated according to Barton & Bandis (1990) for the estimation of the average angle of friction of discontinuities. The estimated angle of friction for the discontinuity planes based on this method was equal to 63 degrees. Slope dip angles were considered equal to 80° and slope orientations were determined from the angle formed between true north and slope face alignment. Slope orientations are as follow: N54° for the NW Slope, N323° for the NE Slope and

N60° for the SE Slope. Software Dips (Rocscience 2004) was used for the stereographic analysis of potential failure modes.

The geomechanical survey was carried out in July 2018 and lasted three days. For this, the scanline method was also used, with red ink markings every five (5) meters, where the RMR values were determined (Bieniawski 1989). The RMR geomechanical classification allows estimating the mechanical quality of the rock mass and the rock support required. The RMR system varies from 0 to 100, and is determined by the sum of six fundamental factors: 1) uniaxial compressive strength of the intact rock; 2) RQD (Rock Quality Designation); 3) spacing of discontinuities; 4) condition of discontinuities; 5) groundwater; and 6) adjustment for discontinuity orientation. For slope applications, Bieniawski (1989) recommend to set the adjustment factor for joint orientation to zero (very favourable condition) and groundwater condition to 15 (completely dry). RMR values close to 0 indicate very poor rock mass quality while high RMR values indicate the opposite (self-supporting rock masses). The uniaxial compressive strength of the intact rock and the joint wall alteration conditions were evaluated according to ISRM (1981). Uniaxial compressive strength tests of rock samples standardized by the Brazilian National Standards Organization - ABNT were also accomplished in the Laboratory of Tests of Construction Materials - LEMAC of the Federal University of Espírito Santo. The RQD parameter was determined according to the equation below, since drill-cores were not available (Palmström 1982):

$$RQD=113-3{,}3.\ J_V \quad (1)$$

Where J_V stands for the number of discontinuities per cubic meter of rock. Joint roughness was determined according to Palmström (1995). For the evaluation of the rock mass quality in the non-sampled areas, RMR values were interpolated by ordinary kriging in the DEMO version of the GS+ software (Robertson 2008). A global variogram direction (omnidirectional) with a tolerance angle of 90° was adopted.

The electrical geophysical prospecting consisted of the use of the DC Resistivity method through the electrical resistivity tomography technique in a Schlumberger electrode array, distributed along six profiles (Figure 1), with five (5) meters of electrode spacing and lengths ranging from 85 to 160 m. Geophysical field data were collected in a single campaign on 11/02/2018. The geophysical equipment used was the Terrameter LS, manufactured by the Swedish company ABEM Instrument, which has a unique automated signal transmission and reception module with 250 W, 1 µV resolution and maximum injection of current of 2.5 A (ABEM 2006). Geophysical field data were processed in the RES2DINV and Oasis Montaj (Geosoft Inc.) softwares and the results were prepared as pseudosections of resistivity (distance x depth) and 3D visualization models.

RESULTS AND DISCUSSION

Results are organized in the following order: structural characterization through the interpretation of pictures of slope faces acquired by drone flyover, kinematic slope stability analysis, geomechanical classification of cut slopes and electrical geophysical prospecting of rock mass.

Drone-based remote sensing for structural mapping

Figure 3 represents the structural interpretation of slope pictures obtained by drone superimposed on the fracture density maps for

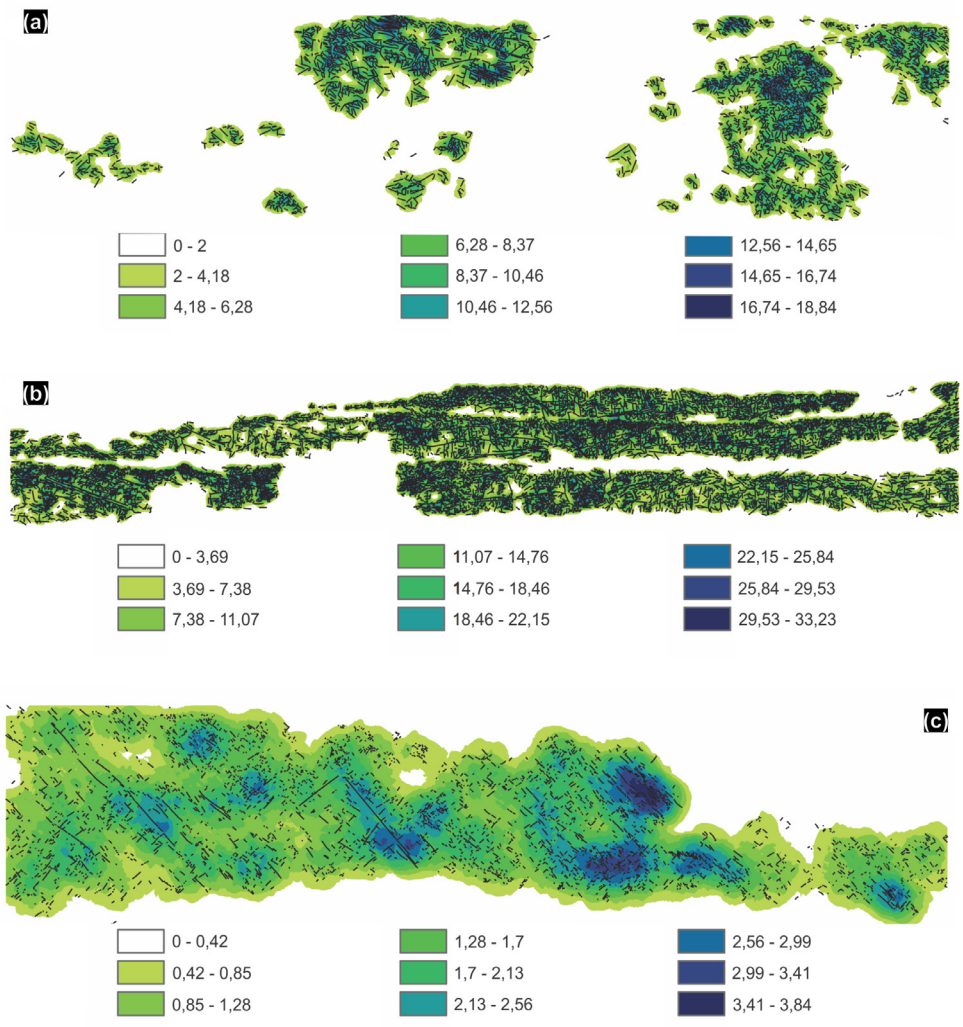

Figure 3. Fracture density map overlaid by structural lineaments interpreted from pictures captured by drone: (a) NW Slope; (b) NE Slope; and (b) SE Slope.

the NW, NE and SE slopes. The interpretation of drone images allowed the recognition of 21,870 fracture traces. Due to the presence of obstacles such as excavation debris, vegetation and/or residual soil, some portions of the slopes were not interpreted.

The NW Slope can be divided into two domains: above and below the ramp main access (Figure 1). In general, fracture traces are linear and have persistences less than 1,5 m. In the zone immediatly above the access ramp, predominate fracture traces dipping to N-NE, which coincide with the orientation of marble banding. In the zone below the ramp, discontinuities have a random pattern. Fracture density values in both domains are very similar.

The NE Slope is the one with the highest density of fractures among all the quarry slopes, but these high values occur as small spots in few places. Bench 1 (lower) can be subdivided into two main domains: center-left and right. The former shows a higher density of fractures with respect to the latter. Additionally, it is noted that in the lower portion of this slope, especially to the left, the density of structures is smaller in comparison with the upper portion. Long traces of discontinuities (5-20 m) are observed in this region. The region of Bench 1 to the right has a density of fracture much smaller than the other

one. In addition, joint traces seem to constrain three discontinuity sets: vertical, horizontal and inclined, dipping approximately 30 - 45° to the right. Bench 2 (middle) can be divided into three domains: extreme left (with small bench heights), center-left and center-right. The center-left domain presents the lowest fracture density values. The center-right region has very fractured rock masses separated by moderately fractured rock masses. Long sub-horizontal curvilinear fracture traces (> 20 m) also occur in this domain and many of them coincide with dikes of metamafic rocks. Bench 3 (upper) has a moderately fractured central domain separated by adjacent very fractured domains. In the central domain, vertical fractures are very striking.

The SE Slope shows a dispersion in the pattern of fracture density along the entire slope, with higher density values concentrated to the right. In general, fracture density is low, and long fracture traces (> 20 m) occur dipping to the right. The SE Slope also shows the lowest values of fracture density in the quarry area.

Rock slope stability assessment by means of kinematic analysis

The kinematic analyzes will be described in the following sequence: planar and wedge, for the slopes NW, SE and NE, respectively. A total of 532 discontinuities were recordered during fieldwork. For the NE Slope, data is organized as follows: Bench 1 (lower), Bench 2 (middle) and Bench 3 (upper). Given the orientation of the NW Slope and the attitudes of the planes of banding, which dip 50° or less to NE, it follows that these structures have no influence on quarry slope instabilities.

Figure 4 shows stereograms for planar failure analysis. As can be seen, a restricted number of planes is located within the risk zone (red hatch). Although these planes could potentially trigger planar failures, it is also necessary to consider their persistence through the slope and the presence of lateral releasing planes. Therefore, it is concluded that this failure mechanism does not interfere quarry slope stability. Nevertheless, a planar failure was observed on the NW Slope, conditioned by a dike of metamafic rock, and another one occur at Bench 2 of the NE Slope (Figure 5).

The conditions for wedge failure happen is much less restrictive than for planar failure. In fact, wedge failures occur in greater number than any other failure mode. Additionally, stereograms reveals higher risk of this type of failure mechanism (e.g. number of intersections of fracture planes within the half-moon shaped risk zone), and varying sliding orientations with dip angles between 64° and 79° (Figures 6 and 7). Among all the slopes analyzed, we highlight the NE Slope, which shows a greater propensity to wedge instabilities. Bench 1 reveals three sets of discontinuities: Fm1 (266/74), Fm2 (230/66) and Fm3 (204/77). The intersections of sets 1 and 2 and 1 and 3 with attitudes 212/65 and 243/73, respectively, are within the zone of risk. Therefore, they are potential candidates of inducing wedge failures. More detailed examination shows that sliding preferentially occur along Fm2, since its dip direction is placed between the line of intersection between fracture sets Fm.1 and Fm.2 and the slope dip direction. The stereograms for Bench 2 reveal six discontinuity sets, and it is the one with greatest amount of intersections within the zone fo risk, with attitudes 239/64, 232/64, 215/79 and 215/64. Note that the intersection with attitude 215/79 has the highest risk for wedge failure since it has the highest dip angle.

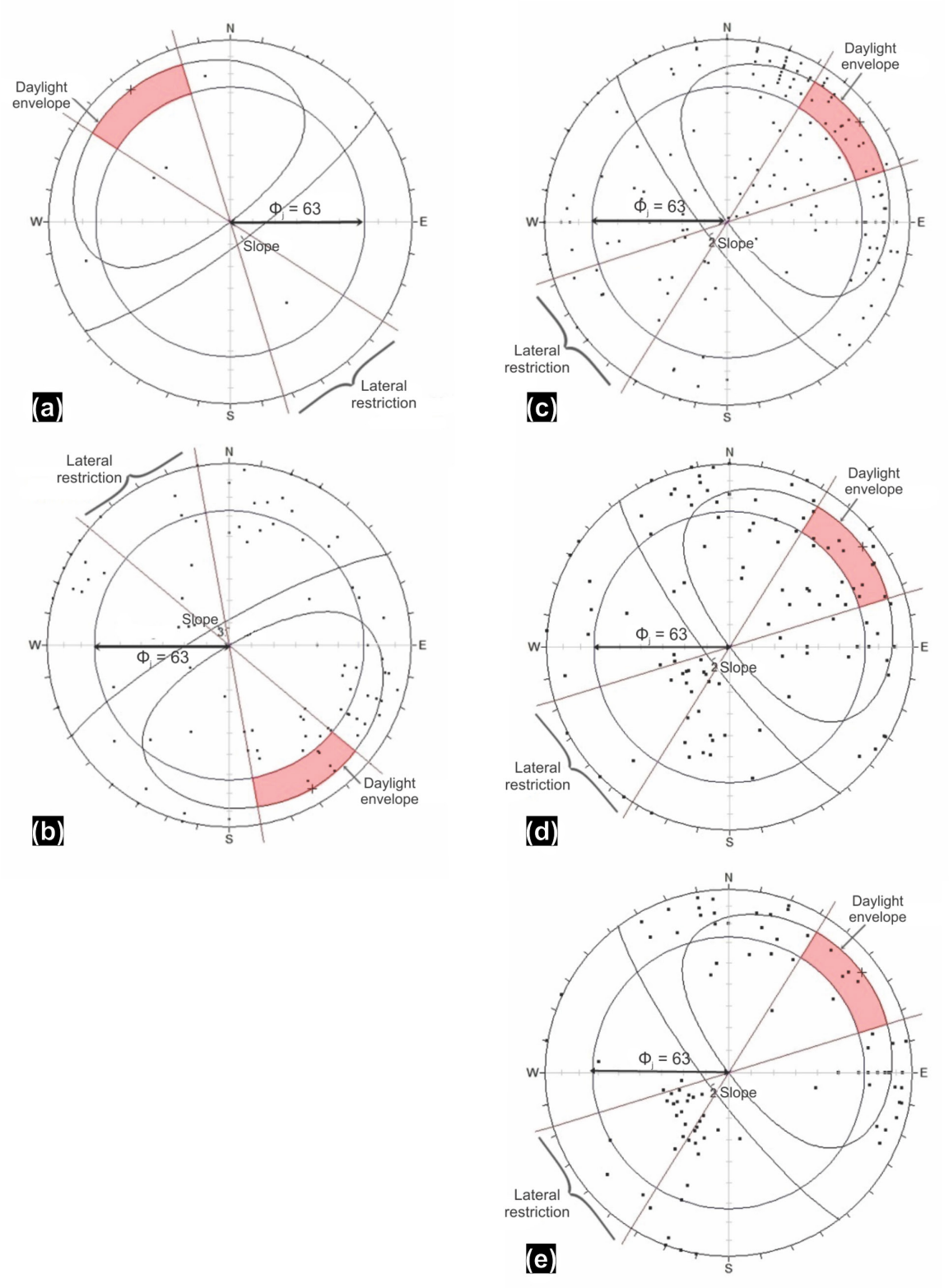

Figure 4. Stereograms for planar slip analysis (poles to planes): (a) NW Slope; (b) SE Slope; (c) NE Slope (Bench 1); (d) NE Slope (Bench 2); and (e) NE Slope (Bench 3). φ_j= angle of friction (friction cone). Lateral restrictions equals to ±20°. The hatched area indicates the critical zone.

Figure 5. Planar failure affecting NW Slope. Slip occurs due to the presence of a dike of metamafic rock 15 cm thick. Note the existence of release joint planes in the upper portion of the slope.

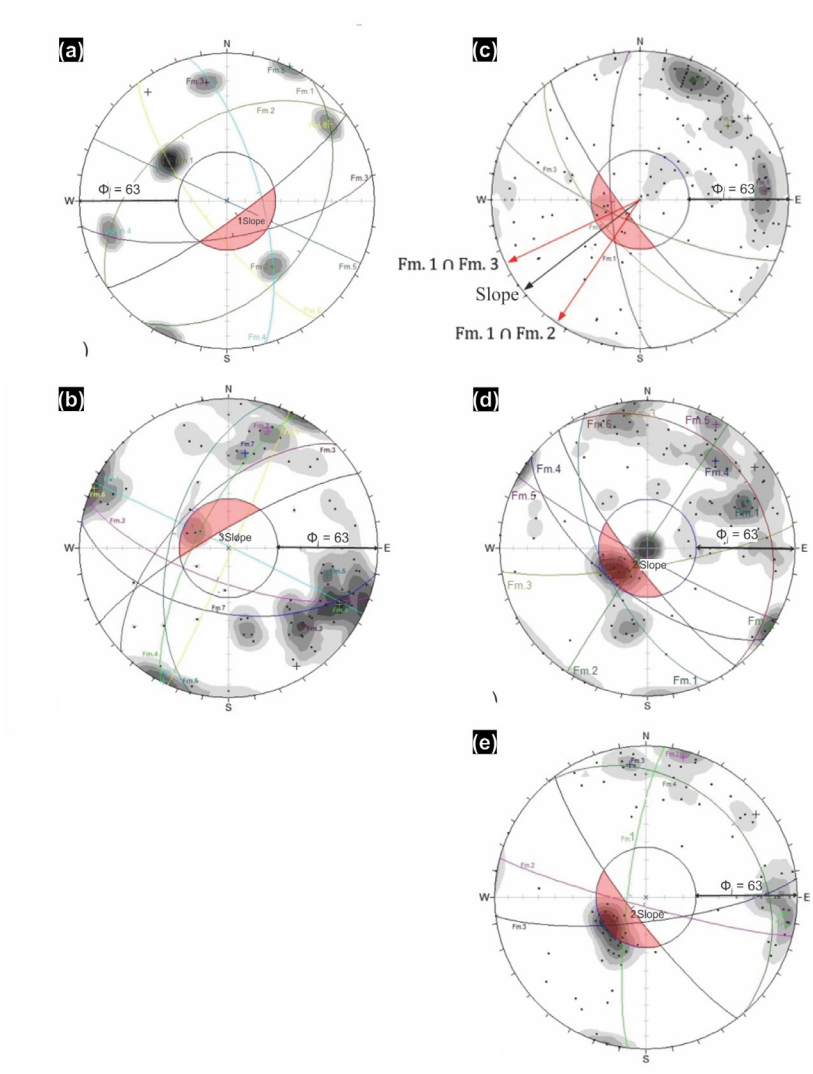

Figure 6. Stereograms for wedge slip analysis (great circles and intersections): (a) NW Slope; (b) SE Slope; (c) NE Slope (Bench 1); (d) NE Slope (Bench 2); and (e) NE Slope (Bench 3). φ_j= angle of friction (friction cone). The hatched area indicates the critical zone.

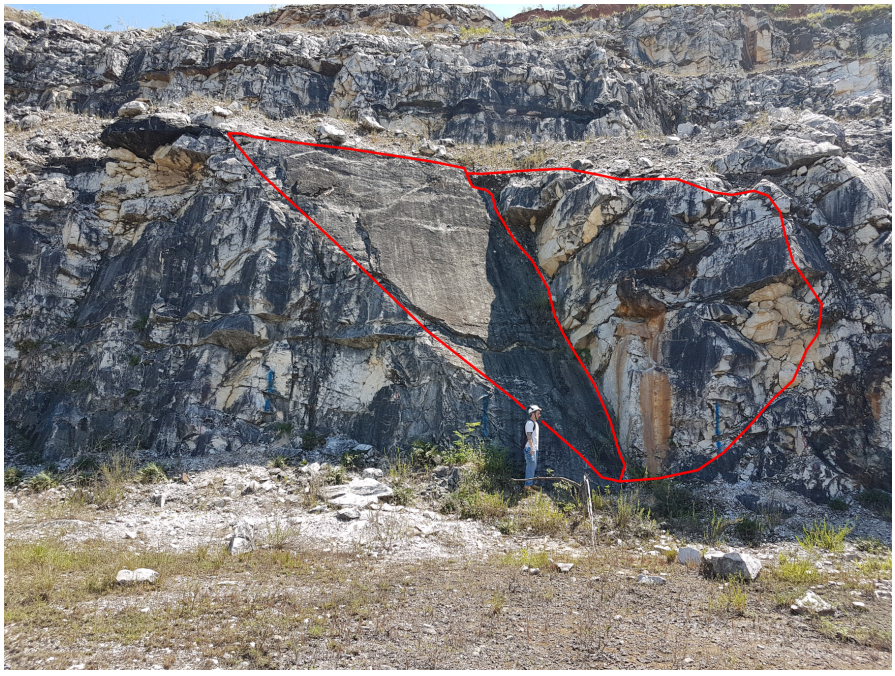

Figure 7. Wedge failure affecting NE Slope (bench 1). Note that slip occurs preferentially in one of the planes.

Geomechanical classification of rock slopes by using the RMR system

Uniaxial compressive strength tests of dry samples of medium-grained marble and dike of metamafic rock confirmed field estimates based on ISRM (1981) (Table I). However, the results obtained for very course-grained marbles reveled strength values well below what was expected. Peng & Zhang (2007) have described similar correlations between grain size and uniaxial compressive strength for layered sedimentary rocks.

The RMR geomechanical classification system was evaluated at 186 discrete points of data collection. RMR isovalues map interpolated by ordinary kriging is shown in Figure 8. The parameters adopted for the exponential model adjusted from RMR values are: range 7.4 m, nugget effect 15.4 m^2 and sill 156.5 m^2. The degree of randomness is considered small and its value is E = 0.109. In the central portion of the quarry area and between the geomechanical survey lines, the interpolated RMR values seem to have been overestimated. For the NE portion of the study area, the interpolated RMR values have no adherence to the field observations since outcrops residual soil. These results are related to the sampling mesh irregularities both in horizontal and vertical (out of plane) domains. Figure 8 also shows that RMR values above 70 (class II - good rock) predominates throughout the quarry.

The NW Slope can be divided into two geomechanical domains. The area to the left shows RMR values between 51 and 64, corresponding to RMR classes II and III (good to moderate rock masses). The domain to the right presents RMR values ranging from 69 to 93, corresponding to RMR classes I and II (very good to good rock masses).

Bench 1 of the NE Slope can also be divided in two geomechanical domains. On the left, predominate RMR values between 70 and 85 (rock mass classes II and I). In the center-right domain, predominate RMR values between 90 and 85 (rock mass class I). In the extreme right portion of Bench 1, RMR values stand

Table I. Results of uniaxial compressive strength tests for some lithotypes found in the study area.

Rock samples	Uniaxial Compressive Strength Tests (MPa)			Average
	1	2	3	
Medium-grained marble	130.48	116.22	127.75	124.82
Very course-grained marble	31.01	37.64	42.26	36.97
Dike of metamafic rock	195.89	219.68	188.34	201.31

Table II. Average values of the RMR parameters for each slope of the study area. Legend: (1) uniaxial compressive strength; (2) RQD; (3) joint spacing; (4) joint persistance; (5) joint aperture; (6) joint roughness; (7) joint infilling; and (8) joint alteration. CV - coefficient of variation.

Slopes	RMR parameters								RMR	CV (%)	Number of stations
	1	2	3	4	5	6	7	8			
NW	10.58	17.83	14.83	3.83	2.42	4.08	6.50	2.50	76.17	28	12
NE (1)	12.00	17.77	16.09	4.17	4.26	3.69	4.94	4.97	83.74	8,7	35
NE (2)	12.00	16.56	13.39	4.02	2.40	3.90	5.05	5.16	78.30	11,8	62
NE (3)	11.66	15.14	11.07	3.36	2.11	3.64	4.95	3.68	70.02	22	44
SE	12.00	16.61	12.73	3.82	2.94	3.48	4.97	3.39	75.57	13	33

around 70 (rock mass class II). In Bench 2, RMR values ranging from 70 to 80 (rock mass class II) predominate. Higher RMR values (= 90) are only verified locally in the center-right domain. In Bench 3 a wide variation in the RMR values is observed. In its left portion, they range from 35 to 60 (rock mass classes IV to III).

The SE Slope has RMR values between 55 and 75 (rock mass classes III to II), being not possible the division in geomechanical domains.

Since RMR values did not show significant dispertion over the entire area as shown in Figure 8, RMR parameters were evaluated based on mean values. Table II summarizes the average values of all the parameters that make up the RMR geomechanical classification system for each one of the quarry slopes. The table reveals that the SE Slope has the lowest RMR values and Bench 3 of the NE Slope the lowest values for most of the parameters. Table II also shows a balanced contribution of each one of the eight parameters to RMR values.

Electrical resistivity tomography for rock mass characterization

The electrical resistivity inversion models for the NE (profiles 1 to 5) and SE (Profile 6) slopes are presented in Figure 9. The profiles indicate geophysical investigation depths of up to 35 m. Apparent resistivity values above 5,000

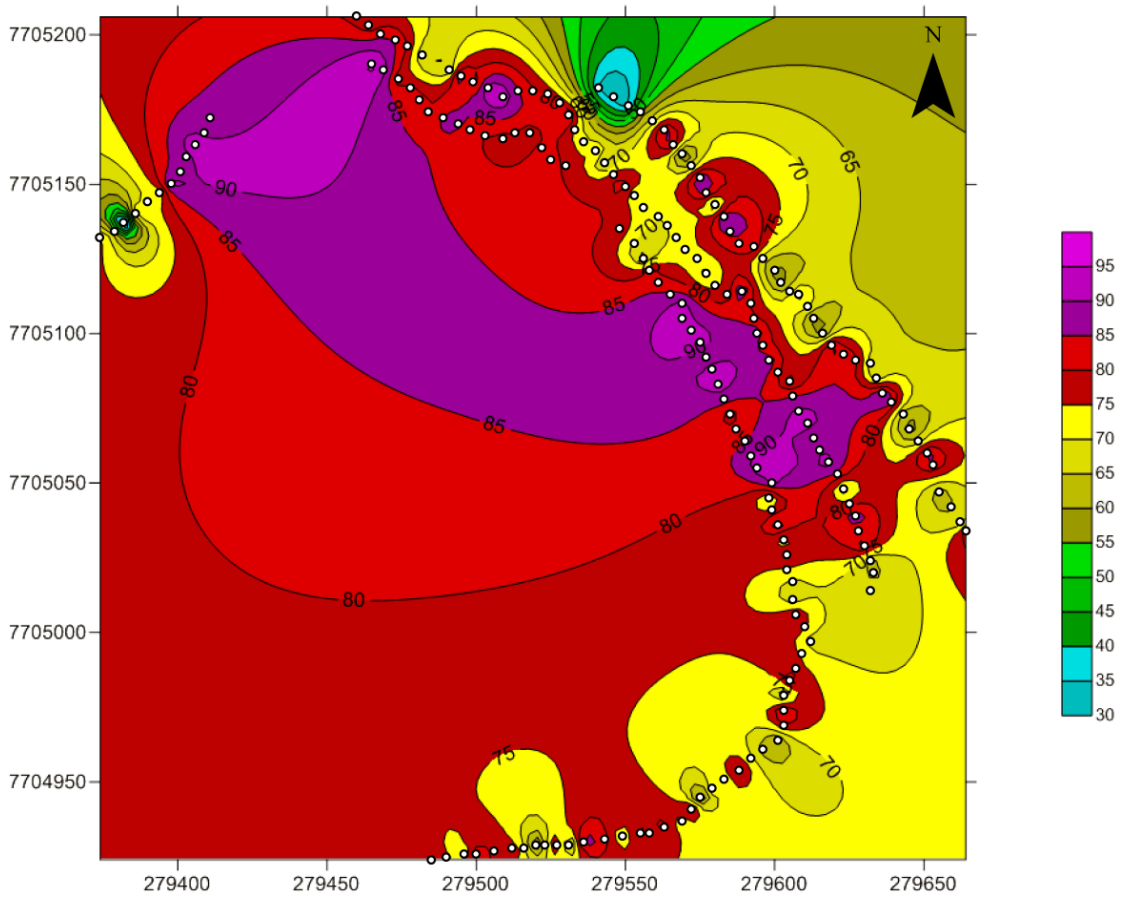

Figure 8. RMR isovalue map generated by ordinary kriging. Blanked dots indicate stations where RMR values were determined.

Ohm.m indicate competent, unfractured and unweathered rock masses, while regions with resistivity values below 200 Ohm.m indicate either soil or water-bearing fractured rock masses.

Profile 1 shows increasing values of apparent resistivity up to the elevation 212 m.a.s.l, where it reaches its maximum (Figure 9a). This depth coincides with the region below the large bench located in the central portion of the quarry (elevation 207 m.a.s.l). The high electrical resistivity values can be interpreted as an undamaged zone (unfractured rock mass), where effects such as brittle tectonic events and rock blasting did not affect rock mass.

Profile 2 shows a large region to the left (below elevation 210 m.a.s.l) with resistivity values over 5,000 Ohm.m (Figure 9b). Increasing electrical resistivity values with depth and an irregular isolines distribution pattern are also observed. The lowest resistivity values (~ 360 Ohm.m) occur in the central portion of the profile (up to elevation 205 m.a.s.l) and indicate a very fractured rock mass. To the right, two small isolated spots of higher apparent resistivity occur. Profile 3 shows a similar pattern than was recorded in Profile 1 (Figure 9c). However, excessively low superficial resistivity values up to the elevation 220 m.a.s.l indicate residual soil, as verified during field survey. Profile 4 shows two large high resistivity nuclei isolated

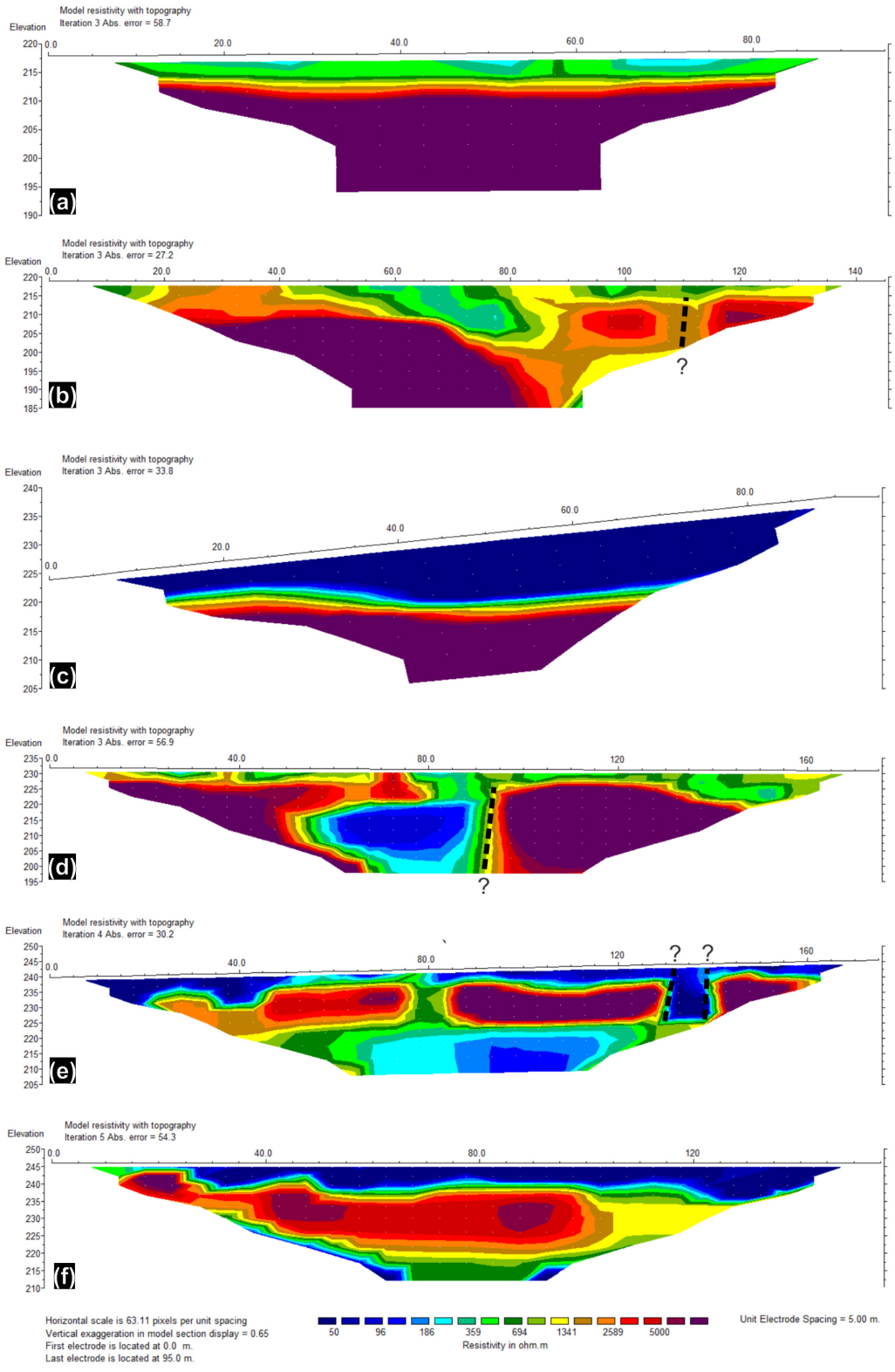

Figure 9. 2D eletrical resistivity imaging pseudosections (Ohm.m): (a) Profile 1; (b) Profile 2; (c) Profile 3; (d) Profile 4; (e) Profile 5; and (f) Profile 6. Profiles 1 to 5 correspond to Slope NE and Profile 6 correspond to Slope SE. Dashed lines indicate interpreted geological faults or dikes.

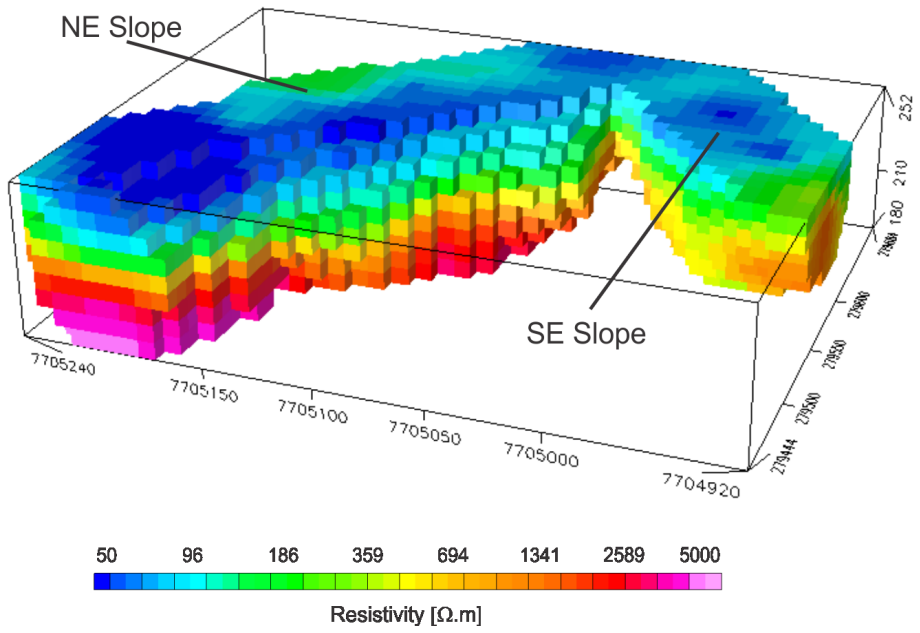

Figure 10. 3D electrical resistivity (Ohm.m) block model for NE and SE slopes.

by a low apparent resistivity zone (Figure 9d). The subvertical distribution pattern of electrical resistivity isolines indicates a dike or a geological fault. Profile 5 reveals superficial low resistivity values followed by a discontinuous horizontal layer (from elevation 237 to 225 m.a.s.l) exhibiting moderate to high resistivity values (> 2,000 Ohm.m) (Figure 9e). In the deepest region of the profile, low resistivity values (< 200 Ohm.m) are observed again and indicates a water-bearing fractured zone. The identation of low resistivity values observed in the right portion of Profile 5 is suggestive of a water-bearing fractured zone or a dissolution cave controlled by geological discontinuities.

Profile 6 reveals that the first five meters is made of residual soil (up to the elevation 240 m.a.s.l) (Figure 9f – SE Slope), confirming field observations. From this depth to approximately the elevation 222 m.a.s.l, a horizontal layer with high apparent resistivities (> 3,800 Ohm.m) occurs. From its base on, the resistivity values decay again. The geophysical prospecting depicted in Profile 6 ends nearly five (5) meters above the slope toe.

The 3D geophysical model of Figure 10 highlights the gradual increase of electrical resistivity with depth. Additionally, it shows that the center-left portion of the NE Slope presents the highest apparent resistivity values, revealing a rock mass with greater chemical and physical integrity.

CONCLUSIONS

This paper describes the integration of different techniques of rock mass characterization for slope stability assessment. The following conclusions are derived from this work:

- Fracture density varies indeed along slope faces; such aspect is well evidenced in the left portion of the Bench 1 of the NE Slope. As geomechanical surveys are usually accomplished at slope toe, this effect significantly affects geomechanical classifications, and consequently slope stability analyzes;

- The number of discontinuities mapped by the scanline survey method represented less than 2.5% of the number of discontinuities traces mapped using high spatial resolution images obtained by drone. This demonstrates that stability analyzes can also be seriously compromised by sampling effect;
- Stereograms revealed a dispersion in the attitudes of the discontinuities, which may be related to blasting effect. In fact, the geophysical Profile 1 revealed a massive and intact rock mass bellow quarry pit floor, where blasting effect is minimal. In addition, the moderate to high angle of friction estimated for the planes of discontinuity may be due to this effect;
- Wedge and planar failure modes are the most critical in the study area, and essentially affect the first two benches of the NE Slope. The mafic rock dikes can also trigger planar sliding as observed in the NW Slope;
- The RMR geomechanical classification system revealed the predominance of rock mass class II (good rock) throughout the quarry area. The RMR values evidenced a general improvement of rock mass quality with depth. This aspect is expected, considering the fact that in tropical regions rock mass upper portions tends to be unconfined and chemically weathered. No clear correlation between low RMR values and wedge/planar failures was found, as rock failures observed during fieldwork are localized and controlled by unfavorable discontinuities (regarding to the orientation, roughness and persistence);
- Banded marbles are defined by the intercalation of bands with different grain sizes. Uniaxial compressive strength tests revealed that the strength of medium-grained marbles are on average at least three times higher than course-grained marbles. This contrast have not been possible to determine by using empirical field methods;
- Geophysical data revealed that the left portion of the NE Slope is made of a competent, massive and unweathered rock mass (> 5,000 Ohm.m). It was also observed that there is a slightly decay in resistivity values from quarry pit floor to top. Such a result converges with RMR values;
- Geophysical pseudosections 4 and 5 showed water-bearing fractured zones that may have been amplified by rock blasting effects (< 200 Ohm.m). These damaged zones may be redirecting groundwater flow into the mine;
- The electrical resistivity tomography has proved to be an important tool for quarry exploitation, since it allows identifying subsurface fractured zones, and therefore, could be used as a guide for quarry prospecting and blast planning;
- No clear correlation between joint density maps and electrical resistivity profiles was observed, which might be related to slope orientation bias and by blasting effects. Joint maps were based on fracture trace mapping interpreted from drone oblique pictures, while geophysical profiles were performed over the quarry benches, where the blasting effects tend to be more reduced.

Acknowledgments

The authors would like to thank Dr. Geilma Lima Vieira, coordinator of the Laboratório de Ensaios em Materiais de Construção - LEMAC of the Universidade Federal do Espírito Santo for the accomplishment of uniaxial

compressive strength tests of rock samples. The authors acknowledge the INOVA DRONES Company, in particular the geologist Hérick Moulin de M. S. Ribeiro, for the acquisition and processing of drone data. The authors thank the geologist Leandro Ribes de Lima (Geomechanics Manager of Leagold Mining, Brazil) for helping with the stereographic projections. The authors thank the undergrad students Garion Guidoeti de Souza dos Santos and Ramirys Lima dos Santos from the Universidade Federal do Espírito Santo - UFES for helping the authors with the geophysical survey.

REFERENCES

ABEM. 2006. Terrameter SAS 4000 / SAS 1000 Instruction Manual.

ABIROCHAS - ASSOCIAÇÃO BRASILEIRA DA INDÚSTRIA DE ROCHAS ORNAMENTAIS. 2018. Disponível em: <http://abirochas.com.br/wp-content/uploads/2018/06/Panorama/Producao_Brasileira_Lavra_b.pdf>. Acessado em: 15/12/2018.

ALEJANO LR, VEIGA M, PÉREZ-REY I, CASTRO-FILGUEIRA U, ARZÚA J & CASTRO-CAICEDO AJ. 2017. Analysis of a complex slope failure in a granodiorite quarry bench. Bull Eng Geol Environ 78: 1209-1224. https://doi.org/10.1007/s10064-017-1160-y.

BARTON N, LIEN R & LUNDE J. 1974. Engineering classification of rock masses for the design of tunnel support. Rock Mechanics 6(4): 189-236.

BARTON NR & BANDIS SC. 1990. Review of predictive capabilities pf JRC-JCS model in engineering practice. In: Rock Joints, Proc int symp on rock joints, Loen, Norway (Barton N and Stephenson O Eds.), p. 603-610.

BASAHEL H & MITRI H. 2017. Application of rock mass classification systems to rock slope stability assessment: a case study. J Rock Mech Geotech Eng 9: 993-1009.

BIENIAWSKI ZT. 1989. Engineering rock mass classification – A complete manual for engineers and geologists in mining, civil and petroleum engineering. Nova York: Wiley Interscience, p. 251.

CARRIÈRE SD, CHALIKAKIS K, SÉNÉCHAL G, DANQUIGNY C & EMBLANCH C. 2013. Combining electrical resistivity tomography and ground penetrating radar to study geological structuring of karst unsaturated zone. J Appl Geophy 94: 31-41.

CARROZZO MT, LEUCCI G, MARGIOTTA S, MAZZONE F & NEGRI S. 2008. Integrated geophysical and geological investigations applied to sedimentary rock mass characterization. Ann Geophys 51(1): 191-202.

CHAMBERS JE ET AL. 2015. Spatial monitoring of groundwater drawdown and rebound associated with quarry dewatering using automated time-lapse electrical resistivity tomography and distribution guided clustering. Eng Geol 193: 412-420.

DAILY W, RAMIREZ A, BINLEY A & LABRECQUE D. 2005. Electrical resistence tomography - theory and practice. In: Butler DK (Eds). Near-Surface Geophysics. Investigations in Geophysics (Book 13). 1st Edition. Vicksburg, US: Society of Exploration Geophysicists, p. 573-598.

EL-NAQA A. 1994. Rock mass characterization of Wadi Mujib dam site, Central Jordan. Eng Geol 38(1-2): 81-93.

ESRI. 2015. ArcGIS Desktop: Release 10.4. Redlands, CA: Environmental Systems Research Institute.

GOODMAN RE. 1980. Introduction to rock mecnhanics. New York: J Wiley & Sons, 478 p.

GYENGE M & HERGET G. 1977. Pit Slope Manual Chapter 3 – Mechanical Properties: CANMET (Canada Centre for Mineral and Energy Technology, formely Mines Branch, Energy, Mines and Resources Canada), CANMET REPORT 77-12, 87 p. August 1977.

HERGET G. 1977. Pit Slope Manual Chapter 2 – Structural Geology: CANMET (Canada Centre for Mineral and Energy Technology, formely Mines Branch, Energy, Mines and Resources Canada), CANMET REPORT 77-41, 123 p. October 1977.

HOEK E & BRAY JW. 1981. Rock slope engineering. London, UK.: E & FN SPON. 3rd Edition, 358 p.

HUDSON JA & HARRISON JP. 1997. Engineering Rock Mechanics: an introduction to the principles. Kidlinggton, Oxford, UK: Pergamon, 444 p.

ISRM - INTERNATIONAL SOCIETY OF ROCK MECHANICS. 1981. Basic geological description of rock masses. Int J Rock Mech and Min Sci 18(1): 87-110.

JORDT-EVANGELISTA H & VIANA DJ. 2000. Mármores da região de Itaóca (ES) e escarnitos no contato com diques máficos e félsicos: mineralogia e petrogênese. Geonomos 8(2): 61-67.

KLICHE CA. 1999. Rock slope stability. Littleton, CO: SME, 253 p.

PALMSTRÖM A. 1982. The volumetric joint count - a useful and simple measure of the degree of jointing. In: Proc. IV Int. Congr. IAEG, New Delhi, p. 221-228.

PALMSTRÖM A. 1995. RMi - a rock mass characterization system for rock engineering purposes. Ph.D thesis, University of Oslo, Norway, 409 p.

PARK H-J, LEE J-H, KIM K-M & UM J-G. 2016. Assessment of rock slope stability using GIS-based probabilistic kinematic analysis. Eng Geol 203: 56-69.

PEDROSA-SOARES AC & WIEDMANN-LEONARDOS CM. 2000. Evolution of the Araçuaí Belt and its connection to the Ribeira Belt, Eastern Brazil. In: Cordani et al. (Eds). Tectonic Evolution of South America, Rio de Janeiro, SBG, p. 265-285.

PENG S & ZHANG J. 2007. Engineering geology for underground rocks. Berlin: Springer, 319 p.

READ J & STACEY P. 2009. Guidelines for open pit slope design. Leiden: CRC, 496 p.

ROBERTSON GP. 2008. GS+: Geostatistics for the Environmental Sciences. Gamma Design Software, Plainwell, Michigan USA.

ROCSCIENCE. 2004. Dips Version 5.1 – Graphical and Statistical Analysis of Orientation Data, Rocscience Inc., Toronto.

ROMANA M. 1985. New adjustment ratings for application of Bieniawski classification to slopes. In: Proceedings of the International Symposium on the Role of Rock Mechanics in Excavations for Mining and Civil Works. Zacatecas: ISRM, p. 49-53.

SANTOS GC & HARTWIG ME. 2018. Geologia da porção norte da Serra de Itaoca-ES. In: 49 Congresso Brasileiro de Geologia, 2018, Rio de Janeiro. 49° Congresso Brasileiro de Geologia. São Paulo: SBG, 2018.

SILVA JND. 1993. Programa de Levantamentos Geológicos Básicos. Cachoeiro de Itapemirim: Folha SF. 24-VAV (Escala 1:100.000). CPRM, 134 p.

TZIAVOU O, PYTHAROULI S & SOUTER J. 2018. Unmanned Aerial Vehicle (UAV) based mapping in engineering geologicalsurveys: Considerations for optimum results. Eng Geol 232: 12-21.

WYLLIE DC & MAH CW. 2004. Rock slope engineering: civil and mining. Suffolk, UK: Spon Press. Forth Edition, 431 p.

How to cite

HARTWIG ME & MOREIRA CA. 2021. Integration of multisources data for quarry slope stability assessment in the Itaoca district (Southeastern Brazil). An Acad Bras Cienc 93: e20190322. DOI 10.1590/0001-3765202120190322.

Manuscript received on March 20, 2019;
accepted for publication on February 17, 2020

MARCOS EDUARDO HARTWIG[1]
https://orcid.org/0000-0002-2661-7506

CÉSAR AUGUSTO MOREIRA[2]
https://orcid.org/0000-0002-6949-6679

[1]Universidade Federal do Espírito Santo, Centro de Ciências Naturais e da Saúde, Departamento de Geologia, Alto Universitário, s/n, Guararema, 29500-000 Alegre, ES, Brazil

[2]Universidade Estadual Paulista, Instituto de Geociências e Ciências Exatas, Departamento de Geologia Aplicada, Av. 24-A, 1515, Caixa Postal 178, 13506-900 Rio Claro, SP, Brazil

Correspondence to: **Marcos Eduardo Hartwig**
E-mail: marcos.hartwig@ufes.br

Author contributions

First author was responsible for data survey and preparation of the manuscript. Second author was responsible for geophysical survey and geophysical data processing.